

Original Article

# Observational study of waves in Hong Kong- Kelvin-Helmholtz waves and stationary mountain waves

Pak Wai Chan<sup>a,\*</sup>, Jielan Xie<sup>b</sup>, Ping Cheung<sup>a</sup>, Chun Kit Ho<sup>a</sup>, Kai Kwong Lai<sup>a</sup>

<sup>a</sup>Hong Kong Observatory, Kowloon, Hong Kong, China

<sup>b</sup>Guangdong Provincial Key Laboratory of Marine Disaster Prediction and Prevention, Shantou University, Shantou 515063, China

## ARTICLE INFO

### Keywords:

LIDAR  
Eddy dissipation rate  
Mountain wave  
Scorer parameter  
Turbulence

## ABSTRACT

Two observed cases of Kelvin-Helmholtz (K-H) waves in Hong Kong have been presented in this paper, based on radial velocity data of a Doppler light detection and ranging (LIDAR) system and from cloud observation. Analysis of atmospheric conditions under which the waves occurred was carried out using ground-based remote-sensing meteorological instrumentation data and simulations on a high-resolution numerical weather prediction (NWP) model. The calculated Richardson number profiles are supportive of the occurrence of K-H waves, while the model simulations for one of the cases reproduced the wave features quite well. The case studies suggest that the advancement of remote-sensing instruments and NWP models reveals the possibility to observe and analyze K-H waves in greater detail. On the other hand, many mountain wave cases near the Hong Kong International Airport (HKIA) are also studied in this paper, namely, the wave-like structure of Eddy dissipation rate, a mountain wave downstream of the terrain on the western side of Lantau Island, and a mountain wave extending to heights near the sea surface. Using the vertical profile of the Scorer parameter based on nearby radiosonde observations, these cases are likely to be stationary mountain waves. The success of NWP simulations in reproducing the mountain wave feature in these cases, however, was mixed. This points to the difficulty of real-time forecasting of mountain waves that may have operational implications for airport operations due to the disrupted airflow.

## 1. Introduction

Kelvin-Helmholtz (K-H) waves usually occur in stratified flows in the presence of significant wind shear, normally manifesting themselves as billows of clouds in the sky. As one of the sources of in-flight turbulence (Storer *et al.*, 2019), understanding of atmospheric conditions under which K-H waves form is important for aviation safety. Located on the coast of southern China in a subtropical latitude, the number of reported cases of K-H waves in Hong Kong has been rather limited, with past cases normally based on visual reports of wave patterns of the clouds. Analysis of the associated meteorological conditions was also limited by the availability of upper-air observations. For example, upper-air temperature and wind measurements, which are required to determine the critical parameter relating to K-H waves, namely, Richardson number (Ri), are only available a few times a day from radiosonde measurements.

However, with the advancement of remote sensing technology, it is possible to have more observational data of such waves (e.g., Grasmick and Geerts, 2020; Malekmohammadi *et al.*, 2025). This paper will present cases of K-H waves in Hong Kong using a multi-platform observational approach. First, data from ground-based Doppler light detection and ranging (LIDAR) systems, including the radial velocity component of Doppler LIDARs, are studied. Furthermore, analysis of atmospheric situations under which such waves occur is carried out using vertical temperature profiles of microwave radiometers and

vertical wind profiles from Doppler LIDARs and radar wind profilers. In addition to observations, the potential use of high-resolution numerical weather prediction (NWP) models to simulate the observed K-H waves and analyze the atmospheric background is also explored.

On the other hand, mountain waves are also occasionally observed at the Hong Kong International Airport (HKIA) in a stably stratified boundary layer. Some examples are shown in Chan *et al.* (2022). They are normally seen downstream of the eastern side of Lantau Island to the south of HKIA, with a clear signature in the Doppler velocity fields of the LIDAR at the airport. Given that mountain waves could lead to low-level windshear and turbulence, which may affect airport operations, a better understanding of conditions favoring their occurrence is also of interest. As such, apart from K-H waves, this paper will also discuss some examples of observed mountain waves.

## 2. Materials and Methods

### 2.1 Meteorological equipment and measurements

Two cases of K-H waves, on 12 March and 24 October 2024, as well as three cases of stationary mountain waves, two on 31 January 2025 and one on 10 December 2024, are studied in this paper, using a range of meteorological equipment in the vicinity of HKIA and also in King's Park (KP) Meteorological Station, located in the urban area of Hong Kong.

### \*Corresponding author:

E-mail address: [pwchan@hko.gov.hk](mailto:pwchan@hko.gov.hk) (PW Chan)

Received: 13 February, 2025 Accepted: 02 December, 2025 Epub Ahead of Print: 26 March, 2026 Published: 16 April, 2026

DOI: 10.25259/JKSUS\_352\_2025

A number of short-range and long-range LIDARs are installed near the three parallel runways of HKIA, as well as in their vicinity. This paper mainly considers short-range LIDARs located near the western end of the north runway of HKIA (R3W) and Siu Ho Wan (SHW), as well as long-range LIDARs to the south of the north runway (HKG3S) and near the south runway (HKG1). The locations of these LIDARs are shown in Fig. 1. The measurement range of the short-range LIDARs is in the order of 3 to 6 km with a range gate of around 10 to 30 m, and range height indicator (RHI) scans are updated every minute or so. Meanwhile, the long-range LIDARs have a measurement range in the order of 10 to 16 km and a range gate in the order of 100 m. The plan position indicator (PPI) scans, normally at 3 degrees or 6 degrees, are updated every couple of minutes.

In addition, a microwave radiometer is installed at King’s Park to provide temperature profiles every hour, while a wind LIDAR is also installed, providing vertical wind profiles at 10-min intervals.

### 2.2 Numerical modelling studies

A high-resolution NWP model is employed to perform a more detailed study on the atmospheric conditions in selected cases. The model in use is the regional atmospheric modelling system (RAMS) version 6.3 with a horizontal spatial resolution of 40 m and a time step of 10 s. The technical setup of RAMS can be found in Chan et al. (2021). However, in order to have finer model resolution in the vertical in order to resolve the waves, more vertical levels have been added in

the simulations presented in this paper. There are 20 vertical levels below a height of around 1000 m, which have been shown in Fig. 2.

### 2.3 Calculation of wave-related parameters

The presence of K-H waves is identified by the Richardson number  $Ri$ , as determined from the following Eq. (1):

$$Ri = \frac{N^2}{\left(\frac{\partial u^2}{\partial z}\right) + \left(\frac{\partial v^2}{\partial z}\right)} \quad (1)$$

where  $N$  is the Brunt-Vaisala frequency,  $u$  and  $v$  are the horizontal components of the wind, and  $z$  is the height. This quantity is calculated from observational data of a microwave radiometer-LIDAR pair, or from the simulated temperature and wind profiles of NWP models. Some studies have been conducted in the past in Hong Kong (e.g. Chan, 2008) to explore aviation applications of the calculation of  $Ri$ .

As for mountain waves, the Scorer parameter ( $l^2$ ) is calculated to establish heights around which the waves occur, using the radiosonde data at KP, according to the formula (2):

$$l^2 = (N(z)/U(z))^2 - U_{zz}/U \quad (2)$$

where  $N$  is the Brunt-Vaisala frequency,  $U(z)$  is the cross-mountain wind speed profile, and  $U_{zz}$  is the second derivative of  $U$  with height  $z$ .

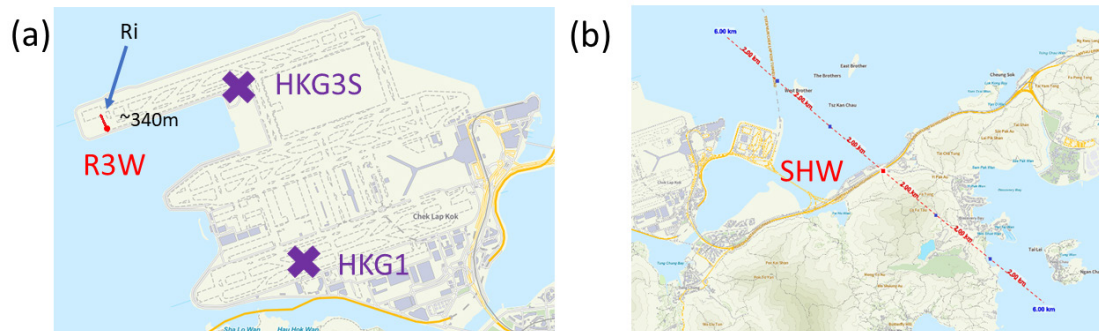


Fig. 1. (a) The location of the short-range LIDAR near the western end of the north runway of HKIA (R3W; red dot) and long-range LIDARs to the south of the north runway (HKG3S) and near the south runway (HKG1). The RHI scanning for R3W is indicated by the red line, while the location for the calculation of Richardson number is indicated by the blue arrow; (b) The location of the short-range LIDAR at SHW and the scanning area.

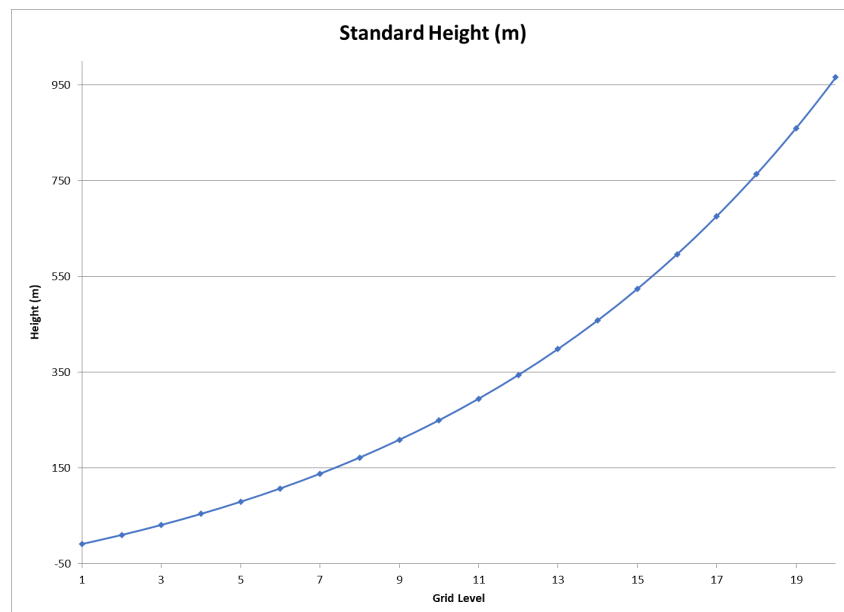


Fig. 2. The heights of the 20 vertical levels of the RAMS model below around 1000 m.

### 3. Cases of Kelvin-Helmholtz wave

#### 3.1 Case 1: K-H wave from doppler LIDAR (12 March 2024)

The first observational case studied occurred at around noon (local time; UTC+8) on 12 March 2024. The K-H wave was observed from the RHI scan of a Doppler LIDAR at R3W. Surface observations from the network of automatic weather stations in the vicinity of HKIA around that time have been shown in Fig. 3. Over the western part of the airport, there were weak and slightly cooler northerly winds, resulting from the weak background northerly winds and the sea breeze. At the same time, east to southeasterly winds prevailed over the rest of the airport and other parts of Hong Kong. Winds from the east or southeast were also observed on higher ground. As such, near the western end

of the north runway, there were northerly winds near the surface, and southeasterly winds aloft.

The Doppler velocity data of the LIDAR at R3W, with a line of scanning that points to the north-northwest (the red straight line annotated in Fig. 1a), indicated K-H waves at multiple time instances. A couple of examples are shown in Fig. 4. The blue color refers to inbound Doppler velocity, which corresponds to northerly flow, while the red color refers to outbound velocity, in this case southeasterly flow aloft. At the interface of the two air masses, many K-H waves showed up nicely. Considering the variation of radial velocity at a constant height of around 1000 m (not shown), the wavelength of such waves was roughly estimated to be in the region of 800 m to 1200 m.

Unfortunately, there were no upper-air temperature observations at HKIA with high enough vertical resolution to calculate the Richardson number. As such, outputs from the RAMS model, which were initialized

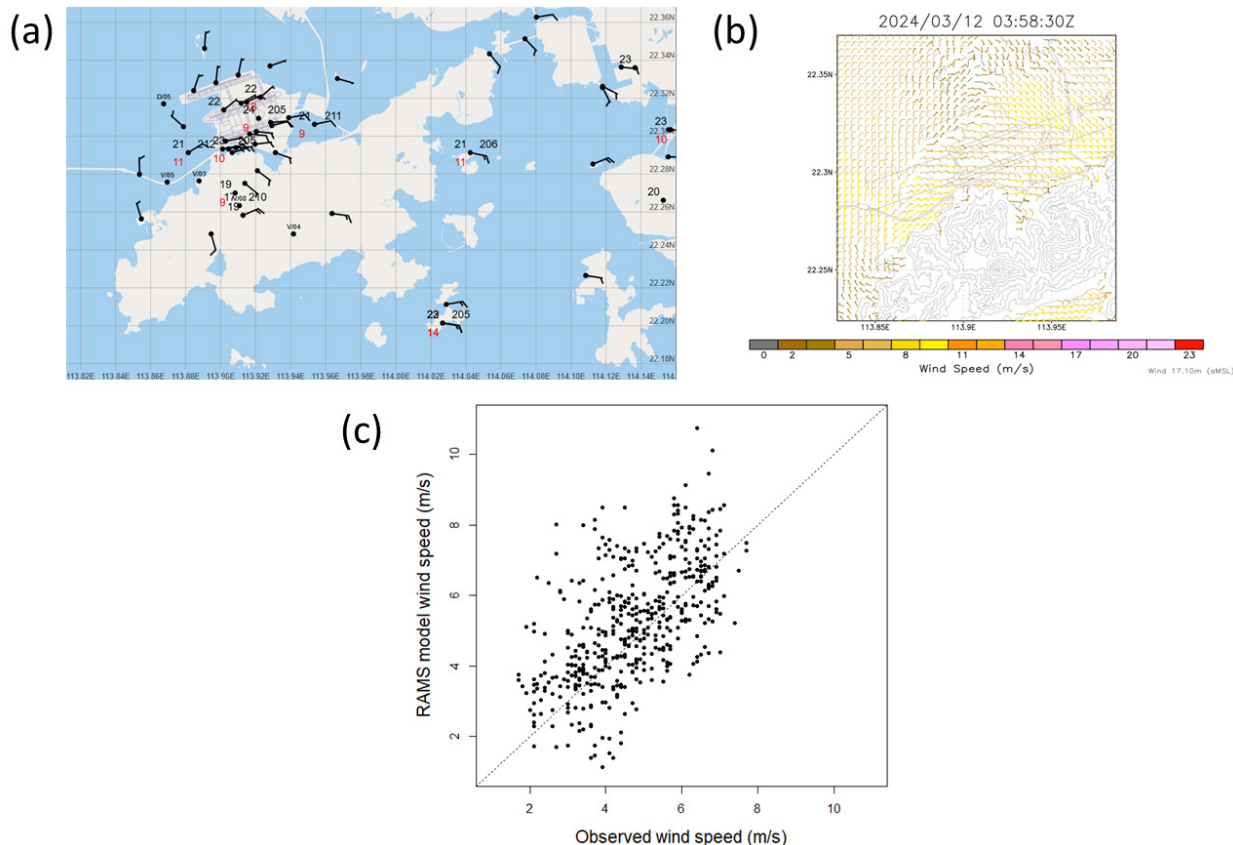


Fig. 3. (a) Surface observations near the HKIA at 03:55 UTC on 12 March 2024; (b) Simulated 10-m wind by the RAMS model at 03:58:30 UTC (11:58:30 Hong Kong local time; HKT = UTC + 8) on the same date; (c) Scatter plot of model wind speed against the observed wind speed at 20 stations which are located within the model domain (refer to panel (b)) and with an altitude of 50 m or below, at 5-min intervals between 03:00 UTC and 05:00 UTC (between 11:00 and 13:00 HKT).

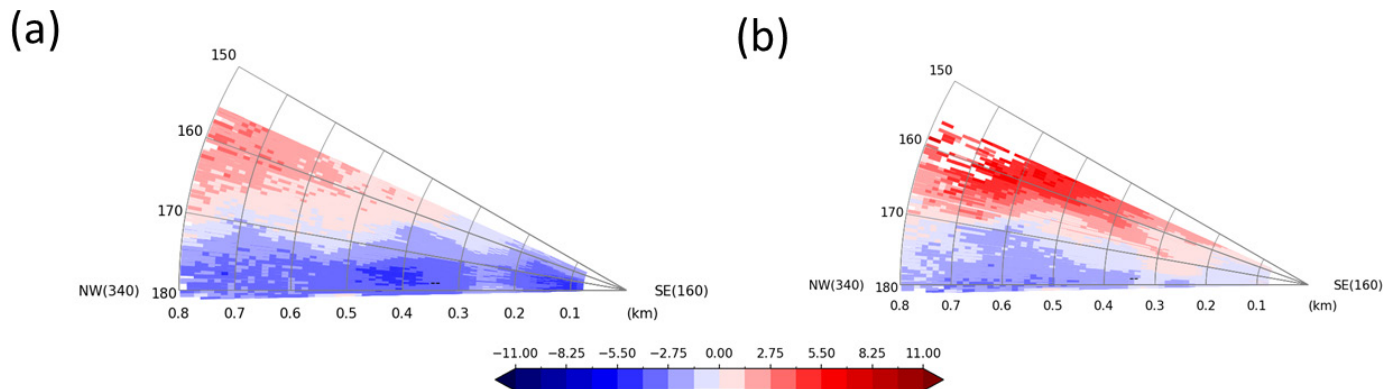


Fig. 4. Doppler radial velocity (in m/s) from the LIDAR at R3W at (a) 03:58:23 UTC and (b) 04:51:41 UTC of 12 March 2024. Negative values (blue) refer to in-bound Doppler velocity, which corresponds to the northerly flow, while positive values (red) refer to out-bound velocity, in this case southeasterly flow aloft.

at 00 UTC, 12 March 2024, for a run of 5 h, were considered to study the waves further. As an evaluation of the NWP results, Fig. 3(b) shows the model-simulated 10-m winds at around the same time as the observations in Fig. 3(a). The general observed wind pattern at the airport was generally well reproduced by the model. Fig. 3(c) shows a scatter plot comparing the observed and modelled wind speed, at 5-minute intervals between 03:00 UTC and 05:00 UTC, at 20 stations which are located within the model domain and with an altitude of 50 m or below. With a correlation coefficient of 0.59 and a mean absolute error of 1.1 m/s, the wind intensity was also reasonably well-simulated.

Fig. 5(a) shows a sample snapshot of the simulated LIDAR RHI scan of Doppler velocity. Many waves were nicely simulated. The one further away from the LIDAR (at 2500 m) resembled features of a K-H wave. Fig. 5(b) shows the  $Ri$  number calculated based on the simulated vertical profiles at the location indicated in Fig. 1(a). Below a height of

around 700 m, the  $Ri$  was generally below 0.25 (red dashed line). As such, based on the model simulation result, the atmospheric condition was supportive of the occurrence of K-H waves.

### 3.2 Case 2: K-H wave from clouds (24 October 2024)

The second case of K-H wave was observed from a picture of clouds (Fig. 6) taken at around 09:46 UTC (17:46H local time; near sunset) on 24 October 2024 at Victoria Harbor, Hong Kong. Wavy clouds with the signature of K-H waves were spotted. Based on the cloud reports from the weather observer at the Hong Kong observatory headquarters near the Victoria harbor, the cloud-base height was around 3500 feet (around 1070 m) at 17:30H and 5000 feet (around 1500 m) at 18:00H.

With the proximity to the Victoria harbor (around 1 km to the north of Hong Kong Observatory headquarters), observations from the wind

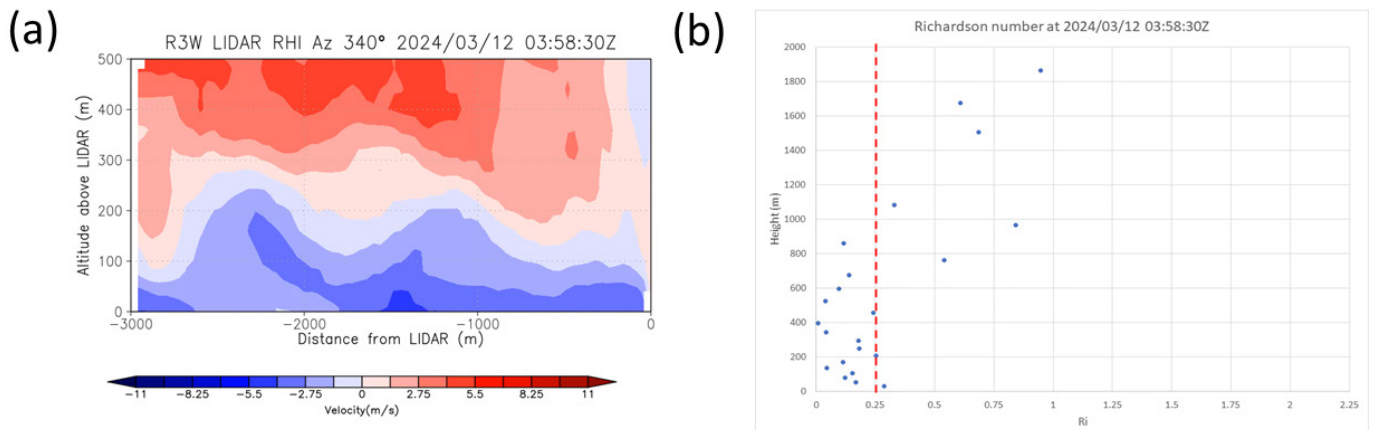


Fig. 5. (a) Simulated LIDAR RHI scan of Doppler velocity from the RAMS model at 03:58:30 UTC on 12 March 2024, which suggests characteristics of a K-H wave; (b) The Richardson number profile (blue dots) at the same time at the location shown in Fig. 1(a) based on the model-simulated vertical profiles.



Fig. 6. Photo taken at the Victoria harbor at 09:46 UTC (17:46H local time) on 24 October 2024, indicating wavy clouds with the signature of K-H waves on the right-hand side of the photo. Courtesy: The Community weather observing scheme (CWOS) of the Hong Kong Observatory, by Mr. Frederick Lau.

LIDAR at King’s Park, which provides vertical wind profiles every 10 min, as well as those from the microwave radiometer, which provides temperature profiles every hour, were studied. From the LIDAR observations, the winds were north to northeasterlies below 2000 m or so above ground, with moderate winds near the surface and reaching strong force aloft (not shown).

Although only hourly temperature profiles are available, considering that under relatively stable weather conditions on the day, the changes in temperature profile within a short period of time would be small. As such, the LIDAR-based vertical wind profile at 17:50H and the radiometer-based temperature profile data at 18:00H, which were the observations closest to the event, were combined to calculate  $Ri$ , and the profile has been shown in Fig. 7. Around the heights of the clouds, namely, around 800 m to 1400 m above sea level, the  $Ri$  was generally below 0.25. It should be noted that the scatter of  $Ri$  at these heights may be related to uncertainties in wind and temperature measurements by the LIDAR and radiometer. Nevertheless, the atmospheric conditions were supportive of the occurrence of the K-H wave.

#### 4. Cases of stationary mountain waves

##### 4.1 Case 3: Wave-like structure of eddy dissipation rate (31 January 2025)

Fig. 8(a) shows an observed wave train which occurred downstream of the eastern side of Lantau Island in a 6-degree PPI scan of the LIDAR on the morning of 31 January 2025, with three wave crests which could be identified. While wave trains on PPI scans are not too uncommon, the novelty of this case is that a wave-like structure also showed up in the map of LIDAR-based eddy dissipation rate (EDR), as given in Fig. 8(b). The EDR map is calculated using the structure function approach (Frehlich and Cornman, 2002), which was also used in previous studies (e.g. Chan, 2011). There were four “blobs” of higher turbulence (moderate turbulence, colored green with a value of around  $0.3 \text{ m}^2/\text{s}^3$ ), against the background of weaker turbulence (colored blue). This wave-like structure of EDR has not been observed at HKIA before. By close

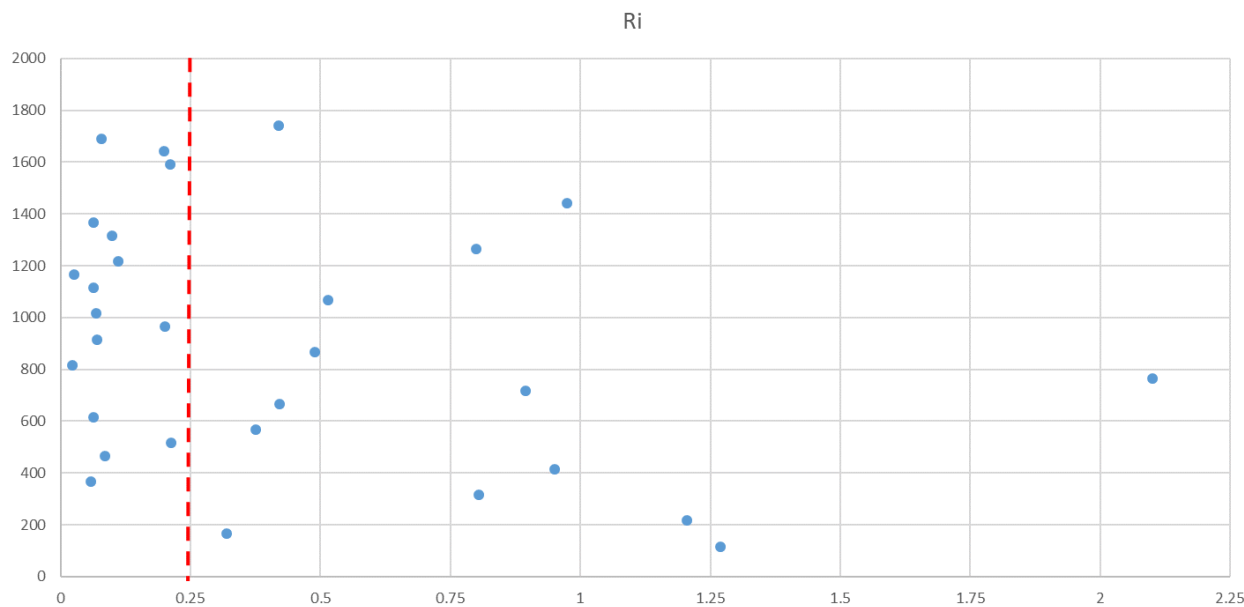


Fig. 7. Profile of Richardson number (blue dots) at different heights (in m) at 09:50 UTC over King’s Park on 24 October 2024, calculated using LIDAR-based observed vertical wind profile and the radiometer-based observed temperature profile data nearest to the time.

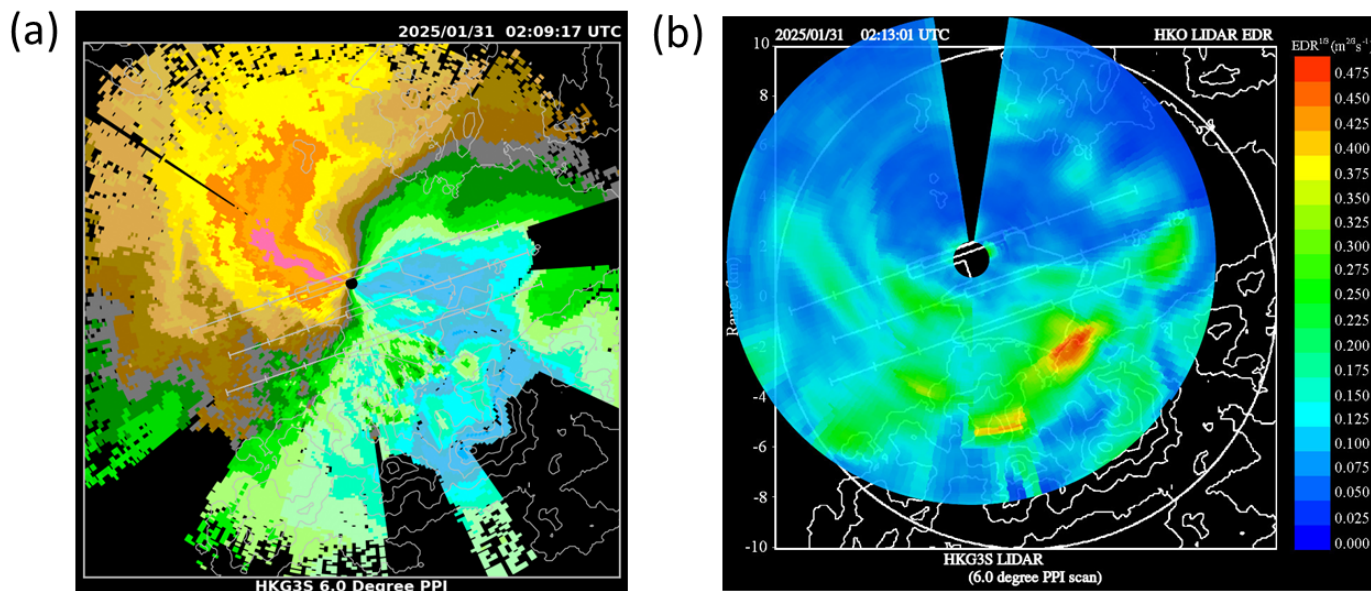


Fig. 8. (a) 6-degree PPI scan of the LIDAR at HKG3S at 02:09 UTC on 31 January 2025; (b) Calculated EDR at around the same time.

inspection, it appears that the moderate turbulence normally occurs near the positions of the wave crests in the Doppler velocity image.

RHI scan of LIDAR provides some insights into the vertical structure of the wave, as provided by the short-range LIDAR at SHW, whose location and scanning pattern could be found in Fig. 1(b). Details about this LIDAR and the RHI scan applications could be found in Chan et al. (2024). The measurement range is up to about 6 km from this LIDAR. A sample RHI scan image has been shown in Fig. 9(a). A wave crest could be observed in this RHI scan, with weaker winds beneath.

The radiosonde data at 00 UTC, 31 January 2025, at King’s Park were analyzed with the calculation of the Scorer parameter, as shown in Fig. 9(b). The parameter showed a decreasing trend from a height of around 400 m up to 800 m above sea level, suggesting conditions favorable for wave energy being trapped in the lower atmosphere. This height range is also consistent with the altitudes over which the mountain wave was observed.

An effort has been made to simulate the mountain wave using RAMS, as initialized at 23 UTC, 30 January 2025, and running for 3 h. Sample model outputs have been shown in Fig. 10. From Fig. 10(a), two wave crests could be reproduced, by the second wave crest downstream of Lantau Island already has rather weak signature, as also shown in the vertical velocity plot of Fig. 10(b). As a result, only the first “blob” of moderate turbulence showed up nicely (Fig. 10c). The second wave downstream is already rather weak and transient. The RHI scan image was also simulated, as shown in Fig. 11, in which the wave crest showed up rather nicely.

Based on radiosonde-based Scorer parameter and numerical simulation results, it is quite well-established that the observed pattern of LIDAR Doppler velocity and EDR is indeed a mountain wave. In this case, a high-resolution numerical weather simulation could reproduce some features well, but the wave appeared to dissipate rather quickly downstream of the mountain in the simulation.

#### 4.2 Case 4: “Blobs” of weaker winds downstream of the western side of Lantau Island (31 January 2025)

The mountain waves observed in HKIA region are mostly downstream of eastern side of Lantau Island. However, waves are sometimes observed downstream of the western side of the island, as shown in the PPI scan of the LIDAR at HKG1 in the evening of 31 January 2025, the same date as Case 3 (Fig. 12a), in which the waves appeared in the form of “blobs” of weaker wind with near 0 m/s Doppler velocity (in grey). Fig. 12(b) shows the calculated profile of the Scorer parameter based on radiosonde data at 12 UTC, 31 January 2025 at King’s Park. The parameter decreased with height from 200 m up to 1200 m above sea level, which was consistent with the occurrence of mountain waves as observed in the LIDAR.

This mountain wave is simulated using RAMS as initialized at 10 UTC, 31 January 2025. From the simulated Doppler velocity field (Fig. 13a), two blobs of weaker winds (in grey, around 0 m/s Doppler velocity) could be found to the west of HKIA. Compared with the simulated vertical velocity field (Fig. 13b), they appeared to occur in regions of updrafts of the mountain wave. Though not three “blobs”

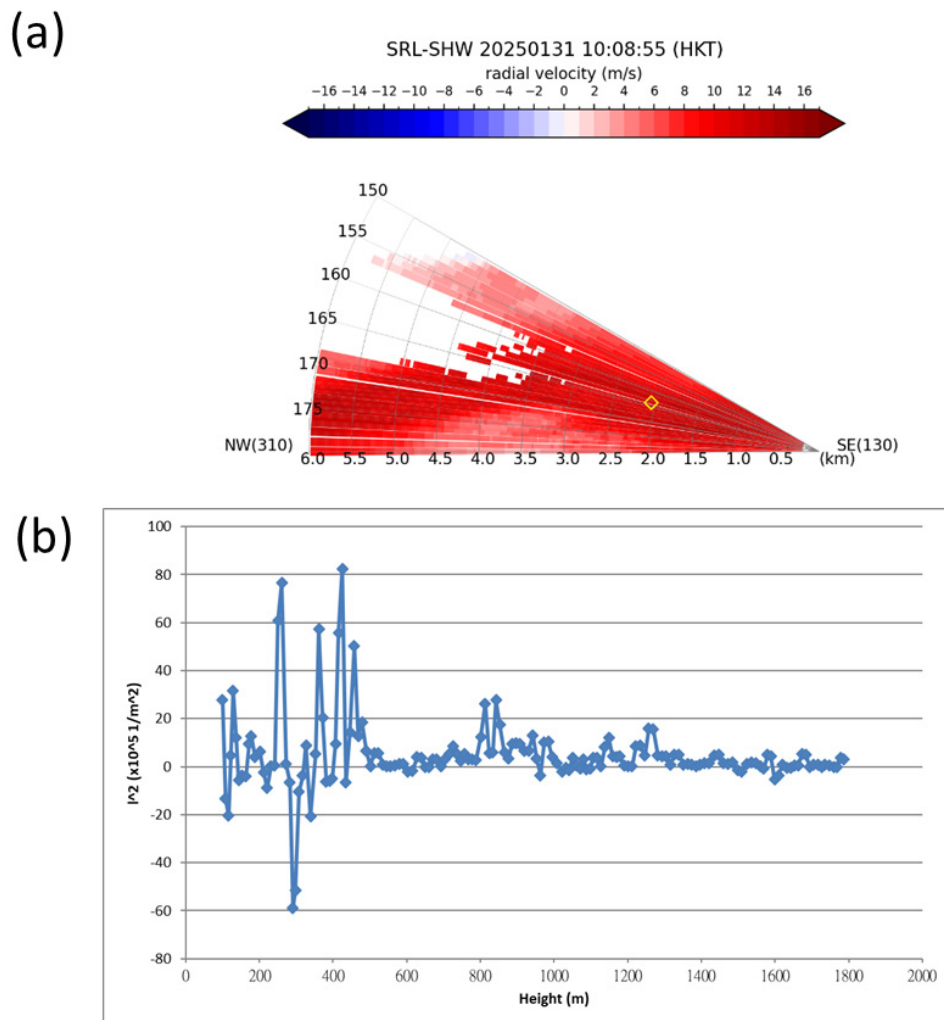
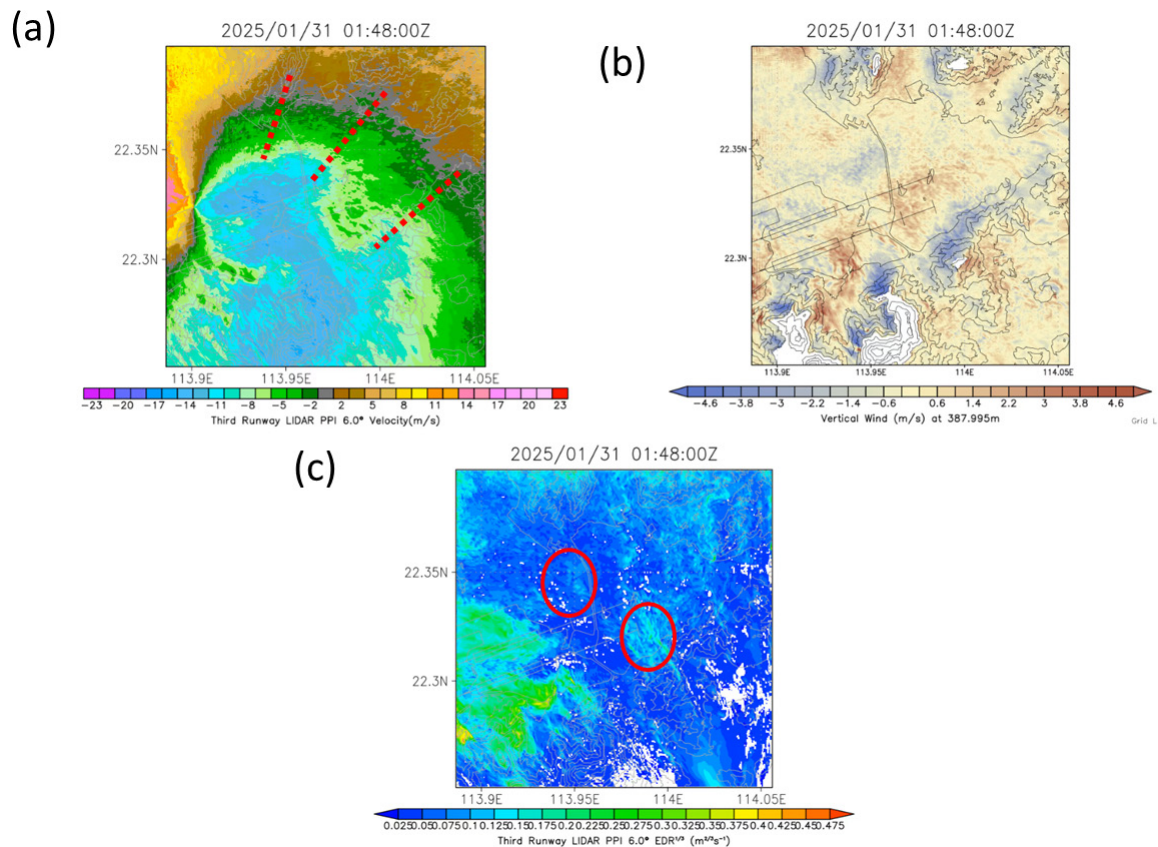
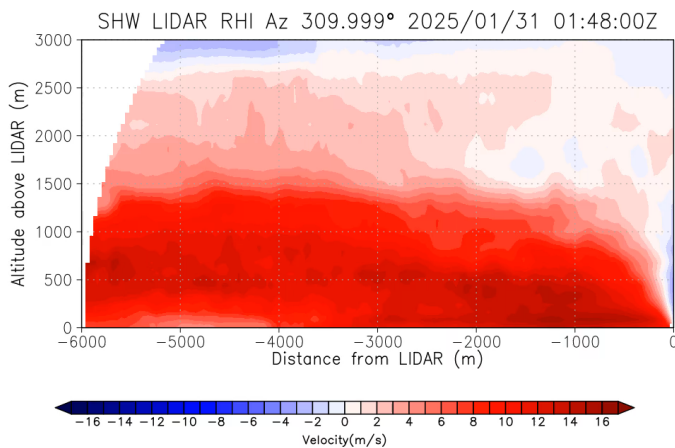


Fig. 9. (a) Radial velocity from the RHI scan of the short-range LIDAR at SHW at 02:09 UTC on 31 January 2025; (b) Profile of Scorer parameter based on radiosonde data at 00 UTC, 31 January 2025 at King’s Park.



**Fig. 10.** (a) Simulated 6-degree PPI Doppler velocity image at 01:48 UTC on 31 January 2025 based on RAMS model initialized at 23 UTC, 30 January 2025, with wave crests marked in red dotted lines; (b) Corresponding vertical velocity map and (c) EDR map with blobs circled in red.



**Fig. 11.** The simulated RHI scan image at SHW at 01:48 UTC on 31 January 2025 based on RAMS model initialized at 23 UTC, 30 January 2025.

of weaker winds are found in the simulation result, the NWP model seemed to reproduce the wave feature relatively well in this case.

**4.3 Case 5: Mountain wave extending downwards to heights near the sea surface (10 December 2024)**

In Chan et al. (2022), some mountain waves shown from a higher elevation angle (such as 6 degrees with respect to the horizon), PPI

scans of LIDAR are documented. However, under favorable weather conditions, it is possible for the wave to occur at heights close to the sea surface, though such waves are rather rare. One example, which was observed in the morning of 10 December 2024, has been shown in Fig. 14, from the PPI scans of the LIDAR to the south of the north runway of HKIA (HKG3S) at various elevation angles (namely 2.4, 3.1, and 6 degrees). The wave extended downstream of the mountains on Lantau Island, more than 20 km away, covering the whole airport region, with at least 6 wave crests being clearly identified.

RHI scan of the wave is provided by the short-range LIDAR at SHW, an example of which is shown in Fig. 15(a). It clearly shows two wave crests, with weaker winds occurring beneath. The height of the wave crests is found to be around 300 to 400 m, therefore the wave is believed to be triggered by the mountains on the eastern side of Lantau Island.

The Scorer parameter based on the radiosonde data of 00 UTC, 11 December 2024 at KP is shown in Fig. 15(b). From around 50 m to 400 m above sea level, this parameter had a decreasing trend. This observation is consistent with the occurrence and the height of the waves identified by the various LIDAR observations.

Modelling of this mountain wave train had been conducted using both RAMS and Weather research and forecasting (WRF) models. However, the waves could not be clearly identified in the simulation outputs despite attempts at different turbulence/boundary layer parameterization schemes, and they are not shown in the present paper. This demonstrates the challenges in simulating mountain waves in the vicinity of HKIA, which may be related to limitations of the model, in particular the complex physical processes involved.

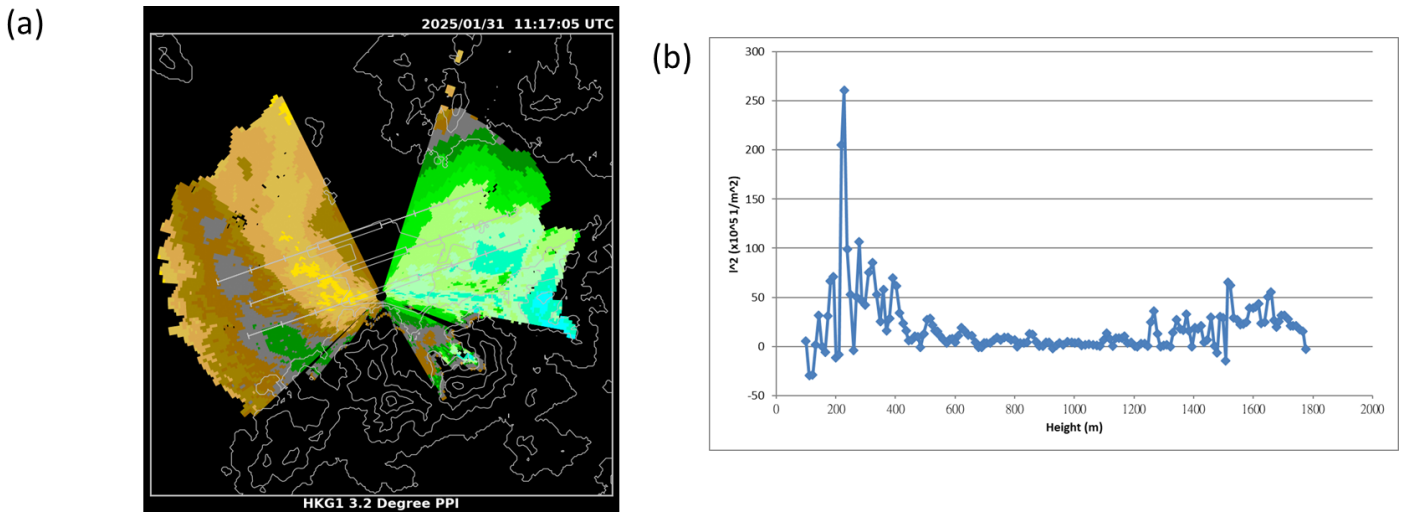


Fig. 12. 3.2-degree PPI scan of the LIDAR at HKG1 at 11:17 UTC on 31 January 2025; (b) Profile of Scorer parameter based on radiosonde data at 12 UTC, 31 January 2025 at King's Park.

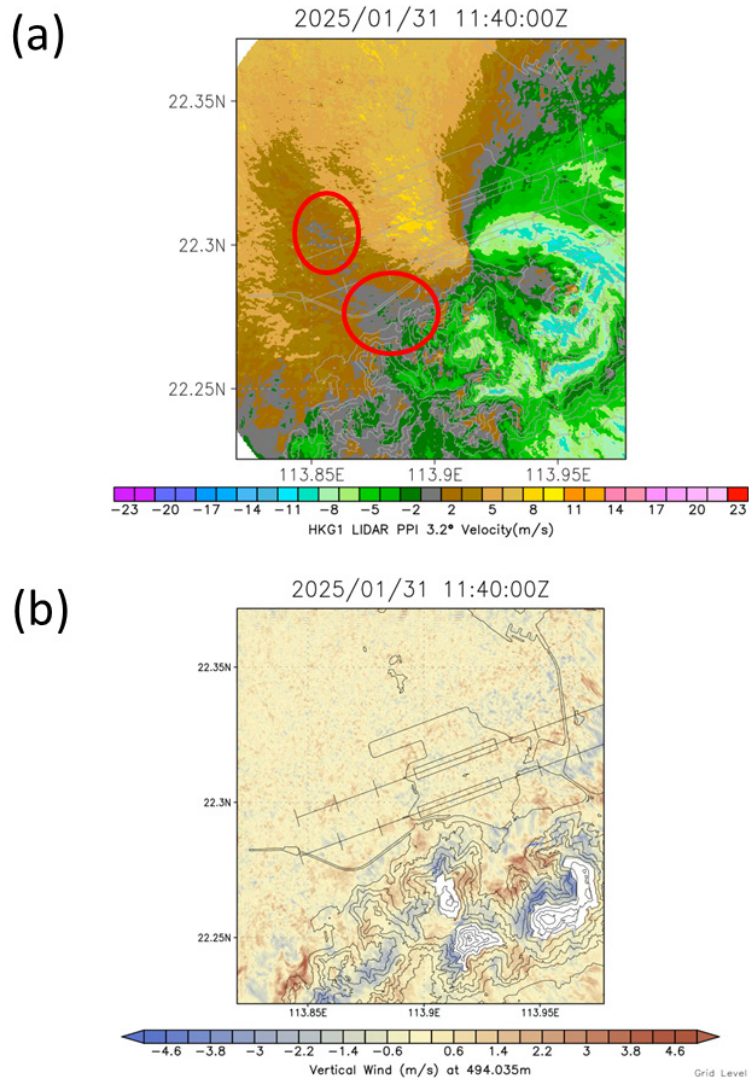


Fig. 13. (a) Simulated 3.2-degree PPI Doppler velocity image at 11:40 UTC on 31 January 2025 based on RAMS model initialized at 10 UTC, 31 January 2025, with “blobs” of weaker winds circled in red; (b) Corresponding vertical velocity map.

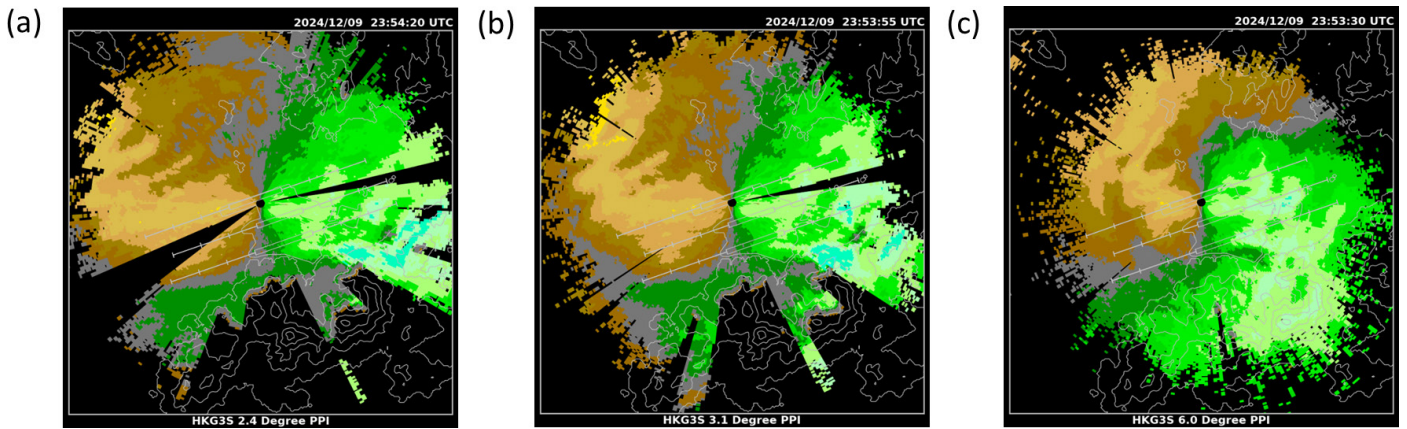


Fig. 14. Doppler velocity image for the PPI scan of the LIDAR at HKG3S at elevation angles of (a) 2.4 degrees, (b) 3.1 degrees and (c) 6 degrees at around 23:54 UTC on 9 December 2024.

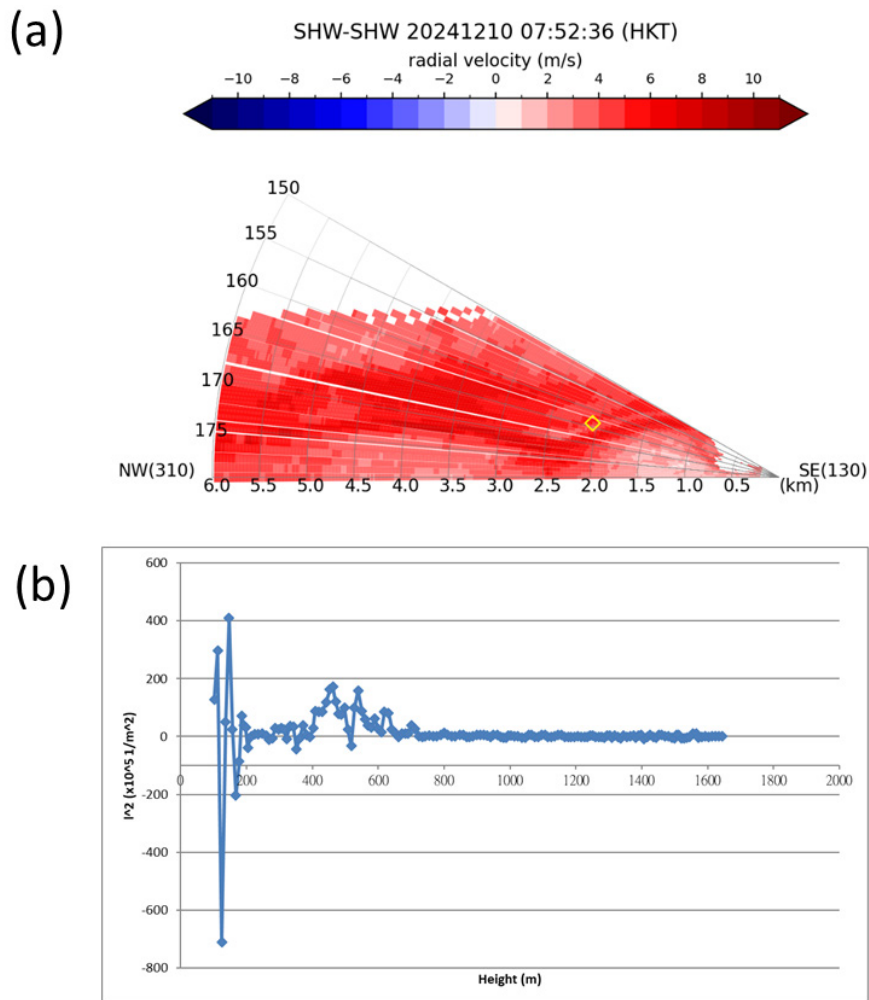


Fig. 15. (a) Radial velocity from the RHI scan of the short-range LIDAR at SHW at 23:52 UTC on 10 December 2024; (b) Profile of Scorer parameter based on radiosonde data at 00 UTC, 11 December 2024 at King's Park.

### 5. Conclusions

A short documentation of two cases of observed K-H waves in Hong Kong is made, namely, from Doppler LIDAR data and from cloud observation. The background atmospheric conditions are analyzed using a multi-platform approach, including microwave radiometer and LIDAR observations, complemented by a high-resolution NWP model.

From the vertical profile of the Richardson number, the atmospheric conditions in the two cases were favorable to the occurrence of K-H waves. These cases demonstrated that the availability of frequently updated upper-air observational data and a high-resolution NWP model opens the possibility of more detailed studies of K-H waves.

This paper also presents three cases of mountain waves that have not been so commonly observed in the HKIA region, including a wave

pattern in EDR, blobs of weaker winds to the west of the airport, and a mountain wave extending close to the sea surface. The occurrence and the height of the waves are generally consistent with the trend of the Scorer parameter calculated from radiosonde data. Numerical simulations have been carried out to evaluate whether the wave features could be reproduced, yet they gave mixed results. While in some cases, the signature of mountain waves could be seen, the number of wave crests and the occurrence of the associated higher turbulence could not be well simulated. In other cases, the wave features could not be clearly identified. These results suggested that the forecast of the occurrence of mountain waves at HKIA, which may have an impact on the airport operation as they are airflow disturbances arising from the mountains and potentially leading to low-level windshear and turbulence, remained a major challenge. While a limited number of cases were considered in this paper, more modelling efforts are being conducted and will be reported in the future.

#### CRedit authorship contribution statement

**Pak Wai Chan:** Conceptualization, investigation, methodology, supervision, writing - original draft. **Jielan Xie:** Formal analysis. **Ping Cheung:** Data curation, investigation, visualization. **Chun Kit Ho:** Formal analysis, visualization, writing - review & editing. **Kai Kwong Lai:** Formal analysis, software, visualization. All authors have read and agreed for the publication of the manuscript.

#### Declaration of competing interest

The authors declare that they have no competing financial interests or personal relationships that could have influenced the work presented in this paper.

#### Declaration of generative AI and AI-assisted technologies in the writing process

The authors confirm that there was no use of artificial intelligence (AI)-assisted technology for assisting in the writing or editing of the manuscript and no images were manipulated using AI.

#### References

- Chan, P.W., 2008. Determination of richardson number profile from remote sensing data and its aviation application. IOP Conf Ser: Earth Environ Sci 1, 012043. <https://doi.org/10.1088/1755-1315/1/1/012043>
- Chan, P.W., 2011. Generation of an eddy dissipation rate map at the Hong Kong International Airport based on doppler lidar data. J Atmospheric Oceanic Technol 28, 37-49. <https://doi.org/10.1175/2010jtecha1458.1>
- Chan, P.W., Lai, K.K., Li, Q.S., 2021: High-resolution (40 m) simulation of a severe case of low-level windshear at the Hong Kong International Airport—Comparison with observations and skills in windshear alerting. Meteorol Appl 28, e2020. <https://doi.org/10.1002/met.2020>
- Chan, P.W., Hon, K.K., Li, Q.S., 2022: Mountain waves near Hong Kong International Airport: Observations and high-resolution model analysis. Weather 77, 20-26. <https://doi.org/10.1002/wea.3878>
- Chan, P.W., Cheung, P., Lai, K.K., 2024: Observation and numerical simulation of terrain-induced airflow leading to low level windshear at the Hong Kong International Airport based on Range-Height-Indicator scans of a LIDAR. Meteorologische Zeitschrift 33, 2024 <https://doi.org/10.1127/metz/2024/1221>
- Frehlich, R., Cornman, L., 2002. Estimating spatial velocity statistics with coherent doppler lidar. J Atmospheric Oceanic Technol 19, 355-366. <https://doi.org/10.1175/1520-0426-19.3.355>
- Grasmick, C., Geerts, B., 2020. Detailed dual-doppler structure of kelvin-helmholtz waves from an airborne profiling radar over complex terrain part I: Dynamic structure. J Atmospheric Sci 77, 1761-1782. <https://doi.org/10.1175/jas-d-19-0108.1>
- Malekmohammadi, S., Cheynet, E., Reuder, J., 2025. Observation of Kelvin-Helmholtz billows in the marine atmospheric boundary layer by a ship-borne Doppler wind lidar. Sci Rep 15. <https://doi.org/10.1038/s41598-025-89554-4>
- Storer, L.N., Williams, P.D. and Gill, P.G., 2019: Aviation turbulence: Dynamics, forecasting, and response to climate change. Pure Appl Geophysics 176, 2081-2095. <https://doi.org/10.1007/s00024-018-1822-0>